One-Dimensional V 2 O 5 /TiO 2 Heterostructures for Chemiresistive Ozone Sensors

Waldir Avansi, Ariadne Catto, Luís F da Silva, Tomas Fiorido, Sandrine Bernardini, Valmor R. Mastelaro, Khalifa Aguir, Raul Arenal

▶ **To cite this version:**

Waldir Avansi, Ariadne Catto, Luís F da Silva, Tomas Fiorido, Sandrine Bernardini, et al.. One-Dimensional V 2 O 5 /TiO 2 Heterostructures for Chemiresistive Ozone Sensors. ACS Applied Nano Materials, 2019, 10.1021/acsanm.9b00578 . hal-02196747

HAL Id: hal-02196747
https://hal.science/hal-02196747

Submitted on 6 Feb 2024

HAL is a multi-disciplinary open access archive for the deposit and dissemination of scientific research documents, whether they are published or not. The documents may come from teaching and research institutions in France or abroad, or from public or private research centers.

L'archive ouverte pluridisciplinaire **HAL**, est destinée au dépôt et à la diffusion de documents scientifiques de niveau recherche, publiés ou non, émanant des établissements d'enseignement et de recherche français ou étrangers, des laboratoires publics ou privés.

One-Dimensional V_2O_5/TiO_2 Heterostructures for Chemiresistive Ozone Sensors

Waldir Avansi Jr.,[*,†] Ariadne C. Catto,[†] Lúis F. da Silva,[†] Tomas Fiorido,[‡] Sandrine Bernardini,[‡] Valmor R. Mastelaro,[§] Khalifa Aguir,[‡] and Raul Arenal[∥,⊥,¶]

[†]Laboratory of Nanostructured Multifunctional Materials, Department of Physics, Federal University of Sao Carlos, UFSCar, Sao Carlos, Brazil 13565-905

[‡]Aix Marseille Université, Université de Toulon, CNRS, IM2NP, Marseille, France 13013

[§]University of Sao Paulo−USP, Sao Carlos, SP, Brazil 13566-590

[∥]Laboratorio Microscopias Avanzadas, Instituto de Nanosciencia de Aragon, Universidad de Zaragoza, 50018 Zaragoza, Spain

[⊥]ARAID, 50018 Zaragoza, Spain

[¶]Instituto de Ciencias de Materiales Aragon, CSIC-U. Zaragoza, 50009 Zaragoza, Spain

ABSTRACT: Over the last decades, there has been considerable interest in the synthesis of one-dimensional (1D) metal oxide nanostructures that can be used in gas sensor devices. Heterostructures, obtained by a combination of different semiconductor nanomaterials with different band energies, have been extensively studied in order to enhance their gas-sensing performance. In this context, our present study focuses on the investigation of chemiresistive-sensing capabilities of a combination of TiO_2 nanoparticles and V_2O_5 nanowires obtained via hydrothermal treatment of the peroxo-metal complex. The formation of V_2O_5/TiO_2 heterostructures was characterized by X-ray diffraction (XRD), transmission electron microscopy (TEM), and X-ray photoelectron spectroscopy (XPS) measurements. This study also proposes an efficient approach to produce 1D V_2O_5/TiO_2 heterostructures with a good range of detection (0.09−1.25 ppm) and remarkable ozone-sensing properties related to repeatability and selectivity.

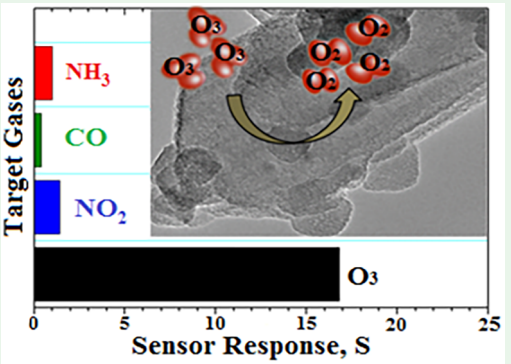

KEYWORDS: *O_3 sensor, V_2O_5/TiO_2, heterostructures, hydrothermal method, chemiresistors*

1. INTRODUCTION

Chemiresistors based on metal oxide semiconducting (MOX) nanostructures have drawn researchers' attentions because of their several advantages related to gas sensor performance, such as stability, sensitivity, and reversibility.[1−5] Despite the fact that SnO_2 and ZnO compounds are the most extensively studied materials used as sensing layer, over the last decades other MOXs have also been studied because of their promising gas-sensing performance, especially their selectivity.[1,2] Vanadium pentoxide (V_2O_5), for example, has excellent properties related to the detection of various (oxidizing and/or reducing) analytes.[6−12] In particular, one-dimensional (1D) V_2O_5 structures (nanowires, nanofibers, nanotubes or nanorods) present enhanced physical and chemical properties, leading to an improvement in their sensing properties.[11,12] Despite having wide-ranging applications, the gas-sensing performance of TiO_2 nanostructures, another MOX, still needs to be better evaluated. TiO_2 in anatase phase has demonstrated interesting sensing properties related to gases such as acetone[13] and H_2S.[14]

A significant effort has been devoted to enhancing the gas-sensing performance of devices based on MOX.[1,2,15−18] In this way, nanostructured heterojunctions, such as WO_3/SnO_2, SnO_2/Fe_2O_3, ZnO/SnO_2, and TiO_2/V_2O_5, have been widely studied because of their satisfactory performance when used in gas sensor devices.[15,19−27] For TiO_2/V_2O_5 compounds, this sensing performance is even better when H_2, CO, NO_2, NH_3, ethanol, ozone, and propane are used.[25,20,19,27] Wang et al. reported an improved ethanol gas sensor employing an MOX based on TiO_2/V_2O_5 heterojunctions with lower operating temperature, faster response/recovery behavior, better selectivity, and a sensor response seven times higher than that found for pristine TiO_2 nanofibers.[20] Fu et al., also studied the gas-sensing properties of V_2O_5/TiO_2 core−shell nanostructures, observing that such materials exhibit superior sensing performance toward NH_3 gas.[19] On the other hand, the gas-sensing properties of V_2O_5−TiO_2 thin films toward analytes

Received: March 28, 2019
Accepted: June 18, 2019

DOI: 10.1021/acsanm.9b00578

such as oxygen, ozone and propane presented a low ozone response attributed to the presence of carbon impurities poisoning active sites on the surface of samples synthesized via sol−gel method.[27] This is expected, since the surface contaminants, such as residual organics or halides from precursors, can poison the surface-active sites in the samples. In this way, the use of a simple and environmentally friendly method to obtain nanostructures without contaminants (organic compounds), for example the hydrothermal treatment of the peroxo-metal complex, appears as an important approach to obtain efficient nanomaterials for gas-sensing purposes.

Among the analytes that demand specific MOX sensors, ozone (O_3) requires special attention, since it is a powerful oxidizing gas that may affect human health if individuals are exposed to subparts per million (subppm) levels.[28−32] Generated by photochemical reactions between sunlight and compounds present in the atmosphere, such as nitrogen oxides (NOx), hydrocarbons, oxygen, and other volatile organic compounds (VOCs), O_3 has been indeed considered an air pollutant with several adverse effects, commonly associated with morbidity and mortality.[29−32] According to the World Health Organization (WHO), O_3 levels from 0.1 ppm (parts per million) in the air can cause pulmonary diseases.[28,29] Additionally, for OSHA (Occupational Safety and Health Administration), the permissible employee exposure to ozone gas is an average concentration of 0.1 ppm for 8 h. Contrarily, the US EPA (United States Environmental Protection Agency) recommends an ozone level of 0.08 ppm for a maximum of 8 h outdoors.[33,34] Therefore, it is desirable to develop sensing materials for devices to detect and continuously monitor O_3 levels present in the atmosphere. In this way, several devices based on WO_3,[35,36] SnO_2,[37] ZnO,[38] Ag_2WO_4,[28] and $CuWO_4$[39] have been studied as a way to detect the ozone level in the atmosphere. Nevertheless, these sensors were reported with a low or unknown selectivity.

As already mentioned, our focus is to develop one-dimensional (1D) V_2O_5/TiO_2 heterostructures obtained by a hydrothermal treatment of the peroxo-metal complex, which was considered a simple and environmentally friendly methodology, and study their gas-sensing performance toward O_3 gas. The properties of V_2O_5/TiO_2 heterostructures were investigated by X-ray diffraction (XRD), X-ray photoelectron spectroscopy (XPS), transmission electron microscopy (TEM), and electron energy loss spectroscopy (EELS). These results have a significant impact on the scientific field due to their potential technological applications.

2. EXPERIMENTAL SECTION

2.1. Preparation of V_2O_5 and V_2O_5/TiO_2 Samples. In a typical procedure to obtain V_2O_5/TiO_2 heterostructures, an appropriate amount of a solution containing V_2O_5 nanowires and titanium (Ti) peroxo complex was prepared. The method employed for both syntheses was described in greater detail by Avansi et al.[8,40,41] and de Mendonça et al.,[42] respectively. The V_2O_5 nanowires were obtained by the dissolution of V_2O_5 micrometric powder (Alfa Aesar, 99.995% purity) in a solution containing distilled water and a proper amount of hydrogen peroxide (H_2O_2 30%), which was set at a molar ratio of 1:10 (V/H_2O_2).[40] Then, the solution was placed into a homemade microcontrolled hydrothermal cell with fine temperature control and self-generated pressure monitoring. The V_2O_5 nanowires were obtained through hydrothermal treatment at 200 °C during 24 h.[40,43] In order to prepare Ti peroxo complex, a specific amount of metallic Ti (99.7%, Aldrich) was added to a solution with H_2O_2/NH_3 (both 29.0%, Synth). Subsequently, a solution containing 200 mg of preformed V_2O_5 nanowires and an appropriate amount of Ti peroxo complex was prepared in order to study three amounts of Ti/V (equal to 5, 10, and 25 mol %) that had their pH value adjusted to around 2. This mixed solution was then placed into a 100 mL hydrothermal cell and subjected to a temperature of 200 °C for a 6 h treatment. The precipitates were separated by centrifugation, washed with pure alcohol for several times, and dried in an electric oven at 50 °C for 24 h.

2.2. Characterization of Samples. The crystalline structures of the as-synthesized samples were investigated using a Shimadzu XRD 6100 diffractometer with a monochromatic Cu kα source, collected in a continuous scan mode (scan speed equal to 2°/min and a step of 0.02°).

The samples were characterized by conventional TEM performed on a Jeol JEM 2010 URP (operating at 200 kV). Additionally, high-resolution (HRTEM) images were obtained by an image aberration-corrected FEI Titan-Cube microscope (operating at 300 kV). Electron energy loss spectroscopy (EELS) measurements were performed on a probe-corrected STEM FEI Titan Low-Base 60−300 (operating at 80KV). HRTEM images and EELS measurements were obtained on a previously described setup.[44]

The XPS analysis was performed on a Thermo Scientific K-Alpha spectrometer using a monochromatic Al Kα source. The as-obtained data were analyzed using Casa XPS software (Casa Software Ltd.a., U.K.), and the spectra were calibrated using a C 1s line (284.8 eV) of the adsorbed C on the sample surface.

2.3. Preparation of the Sensors and Gas Sensor Measurements. The ozone gas-sensing properties of V_2O_5 and V_2O_5/TiO_2 samples were investigated based on a similar procedure already reported by our group.[45,39,28] In the first step, a suspension containing V_2O_5 and V_2O_5/TiO_2 powders in isopropyl alcohol (20 mg/mL) was prepared in an ultrasonic bath for 30 min. Then, it was dripped onto a SiO_2/Si substrate with interdigitated Pt electrode arrays with thicknesses of 100 nm and spaced 50 μm apart. Afterward, the samples were annealed at 500 °C in an electric oven under air atmosphere for 2 h. The sensor sample was then inserted into a gas-sensing chamber to have its temperature and target concentrations controlled[45] Figure S1 presents an image of the dynamic gas-sensing chamber available in our lab. To control the temperature and study the working temperature, the as-prepared sensor was maintained by an external heating source based on an Hg lamp driven by a regulated power supply. As it can be seen in Figure S1, the lamp used for heating was inserted into a metallic platform, avoiding any interaction between light and surface sample. This heating system was able to allow suitable temperature stability and less heat loss to the environment. During the experiments, the electrical resistance was monitored by an electrometer (HP4140B Source/Pico-ammeter) with the application of 1 V DC voltage. Dry air was used both as a reference (baseline) and a carrier, and O_3 gas was generated by oxygen oxidation using a pen-ray UV lamp (UVP company, model 97-0067-01). The total gas flow rate was kept constant and equal to 500 sccm. The gas-sensing performance was available to O_3 concentrations ranging from 0.09 to 1.25 ppm. To investigate the selectivity of the samples, NO_2, CO, and NH_3 gas-sensing measurements were performed at different concentrations in 3 cycles of 60 s. To study the sensor response (S), we employed the same equation already reported by several papers, defined as $S = ((R_{gas} - R_{air})/R_{air})$, where R_{gas} and R_{air} are the electric resistances of the device exposed to gas and dry air, respectively.[45,39,28] Sensor response time and recovery time were also defined as already reported.[45,39,28] The former refers to the time required for the electrical resistance to reach 90% of its initial resistance value, whereas the latter designates the time required for the electrical resistance to recover 90% of its initial value after gas flow interruption. The response and recovery times were estimated using the sensor response upon an exposition time of 5 min. This parameter was chosen because the V_2O_5/TiO_2 sample did not reach the saturation level, even for longer times, as seen in Figure S2.

3. RESULTS AND DISCUSSION

Initially, the as-obtained samples were studied by X-ray diffraction (XRD), as seen in Figure 1. These results confirm

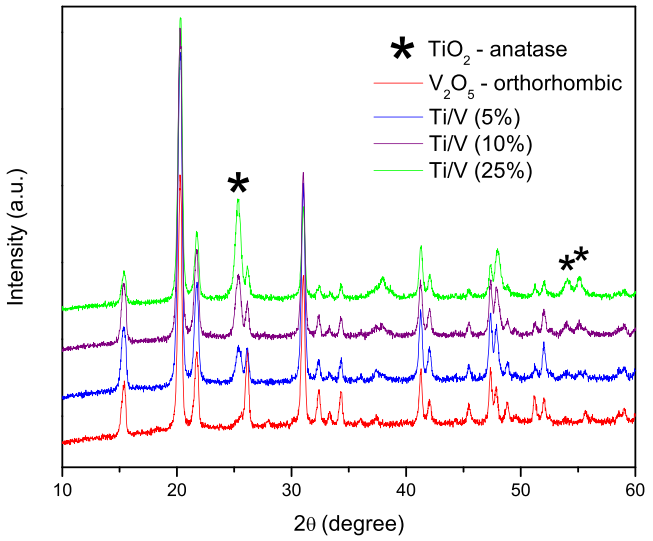

Figure 1. XRD patterns of the as-obtained V_2O_5 and V_2O_5/TiO_2 samples (Ti/V − 5, 10, and 25 mol %) and the reference compounds adopted (V_2O_5 orthorhombic (JCPDS 85-0601) and TiO_2 anatase (JPCDS 21-1272)).

only the presence of V_2O_5 orthorhombic nanostructure (PDF #85-0601)[40] for pristine samples, as expected. For V_2O_5/TiO_2 samples, both V_2O_5 orthorhombic (JCPDS 85-0601)[40] and TiO_2 anatase (JPCDS 21-1272)[42−44] crystalline phases can be observed (denoted by * in Figure 1), especially by the presence of a more pronounced diffraction peak at around 2θ equal to 25°, which has its intensity increased when a higher amount of TiO_2 is added.

Figure 2 corresponds to representative transmission electron microscopy (TEM) images of the as-synthesized samples. They are composed of nanowires decorated with nanoparticles sized around 20 nm, as seen in Figure 2f. As expected, a small amount of such nanoparticles can be visualized for V_2O_5/TiO_2 samples with Ti/V—5 and 10 mol %—according to Figure 2.

Electron energy loss spectroscopy (EELS), when developed in a TEM, is a very powerful technique for investigating the chemical composition of materials at the local (even atomic) level.[46−49] Representative EELS mapping analyses (Figures 3b−d) and HRTEM image (Figure 4) obtained for the V_2O_5/TiO_2 (25 mol %) sample confirm that nanowires and nanoparticles correspond to V_2O_5 and TiO_2, respectively.[40,42] Fast Fourier transform (FFT) analysis from the indicated regions A and B (Figures 4b and c), respectively, validate the single crystalline nature of V_2O_5 orthorhombic and TiO_2 anatase nanostructures. As a matter of fact, the analysis of the interface region reveals the coalescence between the different nanostructures, confirming the formation of V_2O_5/TiO_2 heterostructures. Furthermore, TEM images also show the presence of other nanoparticles attached to different regions of V_2O_5 nanowires, indicating that the growth of heterostructures occurs through epitaxial growth process, similar to what was observed for other heterostructures obtained by hydrothermal method.[52,53] Thus, the growth mechanism appears to be related not only to a specific

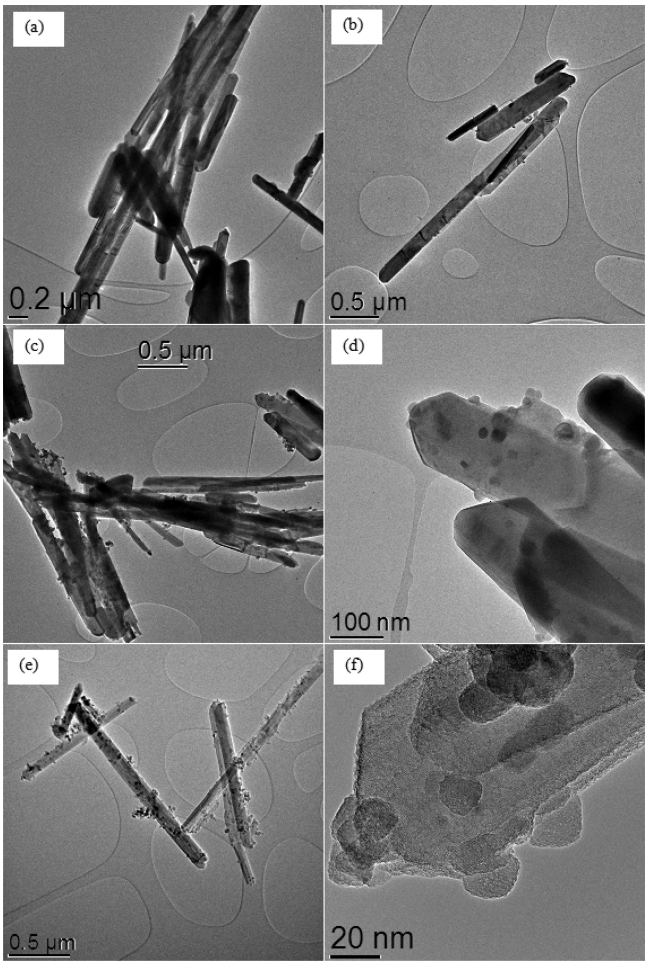

Figure 2. TEM images of V_2O_5/TiO_2 samples with (a and b) Ti/V = 5 mol %; (c and d) Ti/V = 10 mol %; and (e and f) Ti/V = 25 mol %.

crystallographic plane or its respective surface energy but also to the presence of defects on the V_2O_5 surface.

The ozone gas-sensing properties of pristine V_2O_5 and V_2O_5/TiO_2(25 mol %) samples were investigated. First, the optimum working temperature (T_{work}) of the samples was studied through a 5 min exposure to 0.29 ppm of O_3. According to Figure S3 (Supporting Information), the results indicate that the V_2O_5/TiO_2 heterostructure presents a high response compared with the pristine V_2O_5 for all temperatures. Indeed, we found that the best response occurs at 300 °C, as observed in Figure S3. In addition, it can be noted that the sensor response decreases at a temperature above 300 °C, which represents a typical behavior of a metal oxide gas sensor. This can be attributed to a competition between adsorption and desorption processes.[2,16,37,50] Furthermore, both samples present total reversibility and an excellent repeatability, as seen in Figure S4.

Once the optimum working temperature was found, the samples were kept at 300 °C and then exposed to different O_3 levels for 5 min, as shown in Figures 5a and b. It is clear that the response increases when the exposure to O_3 gas starts until reaching a saturation stage, then it decreases to its original value when the injection is switched off. This behavior reveals desirable features for a sensing material, such as good sensitivity, total reversibility, and nonsaturated response.[50,51]

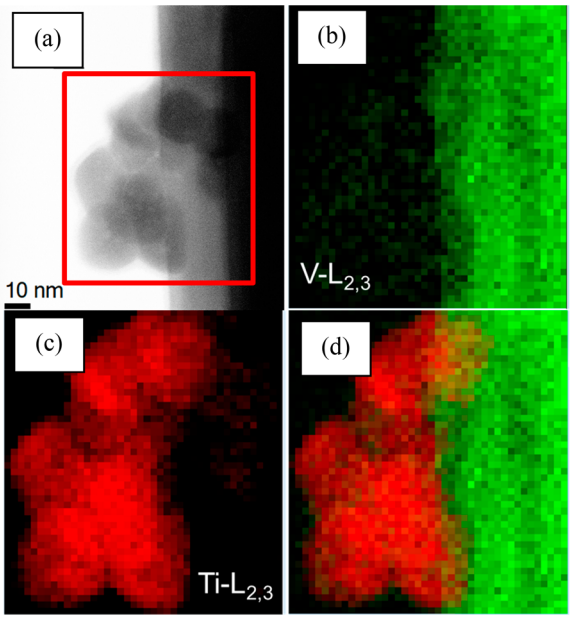

Figure 3. Electron microscopy analysis of V_2O_5/TiO_2 samples: (a) STEM bright-field image of a region containing several nanoparticles on nanowires; (b and c) EELS elemental maps extracted from the EELS spectrum-image recorded in the region showed in a, corresponding to V and Ti, respectively; and (d) combined elemental map of b and c.

Regarding the gas-sensing performance, from Figure 5 it is evident the higher response was presented by the heterostructure in comparison with the pristine sample. This enhancement can be attributed to the presence of additional sites, which are promoted by the formation of a heterojunction. These sites are thermally activated and play an important role in the ozone adsorption process.[16,38,45,52] Zheng and coworkers studied the TiO_2-doped SnO_2 powders employed as gas sensors capable of detecting volatile organic compounds (VOCs). The authors observed that the formation of an n−n junction between both semiconductors become beneficial to oxygen adsorption on the sample surface because of a greater electron density.[53] Furthermore, a linear relationship between sensor response and O_3 level for the V_2O_5/TiO_2 heterostructure is also perceived, suggesting that even a concentration of 1.25 ppm of O_3 is not enough to fill all sites available on the heterostructure surface.

Figure 6a shows the normalized sensor response for both pristine V_2O_5 and V_2O_5/TiO_2 heterojunction upon an exposure to 1.25 ppm of O_3 at a working temperature of 300 °C. The analysis of these dynamic curves reveals that the formation of the heterojunction also affects the adsorption process of the sensing material while its desorption remains unchanged, as seen Figure 6a.

The variation of response and recovery times as a function of O_3 concentration is displayed in Figure 6b. It can be observed that the V_2O_5/TiO_2 heterostructure presents a longer response time than that of the pristine sample. This behavior can be related to a high density of active sites in the heterostructure, which increases the saturation level, and consequently will require longer times to be filled. Regarding the recovery time, the results obtained are quite similar for both samples, since the provided thermal energy is enough for the complete desorption of O_3 molecules adsorbed on the surface of the samples.[38]

The selectivity is another essential parameter to be considered when developing a gas detection device.[2,50,54,55] In this sense, the sensor response of V_2O_5/TiO_2 heterostructures was investigated for oxidizing and reducing gases, i.e., NO_2, NH_3, and CO, as seen Figure 7. The responses of the pristine V_2O_5 and V_2O_5/TiO_2 heterostructure were compared for an exposure of O_3, NO_2, NH_3, and CO gases for 60 s at a working temperature of 300 °C. The values found for the V_2O_5/TiO_2 heterostructure were around S = 1.4 for O_3, S = 0.04 for NO_2, S = 0.06 for CO, and S = 0.03 for NH_3, clearly indicating a high selectivity of heterostructure, which responds

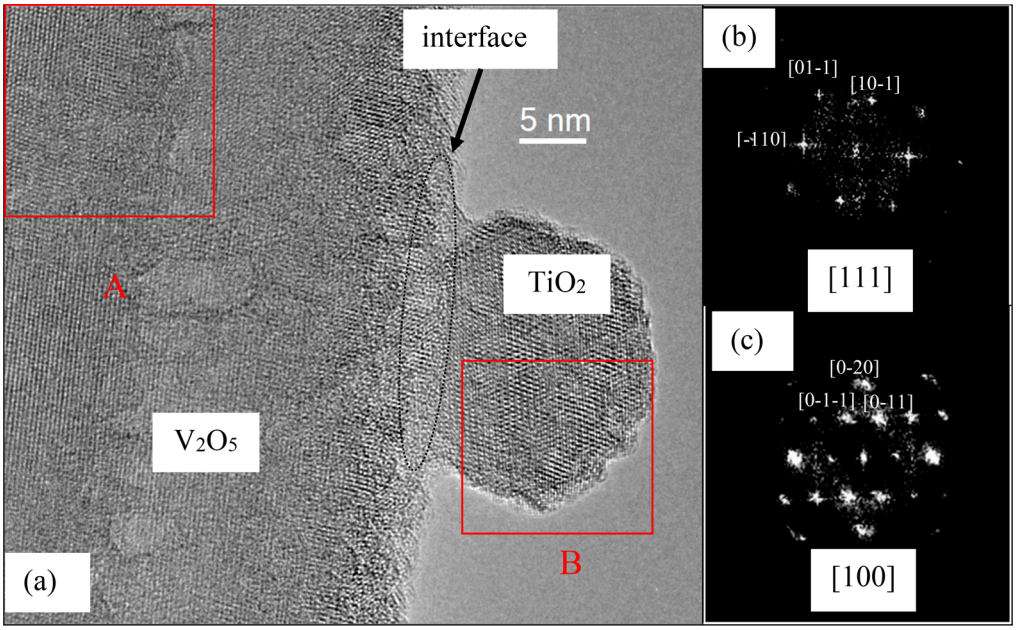

Figure 4. (a) HRTEM image of V_2O_5/TiO_2 heterostructures; (b and c) Fast Fourier transform (FFT) related to the regions (A and B, respectively) illustrated in a.

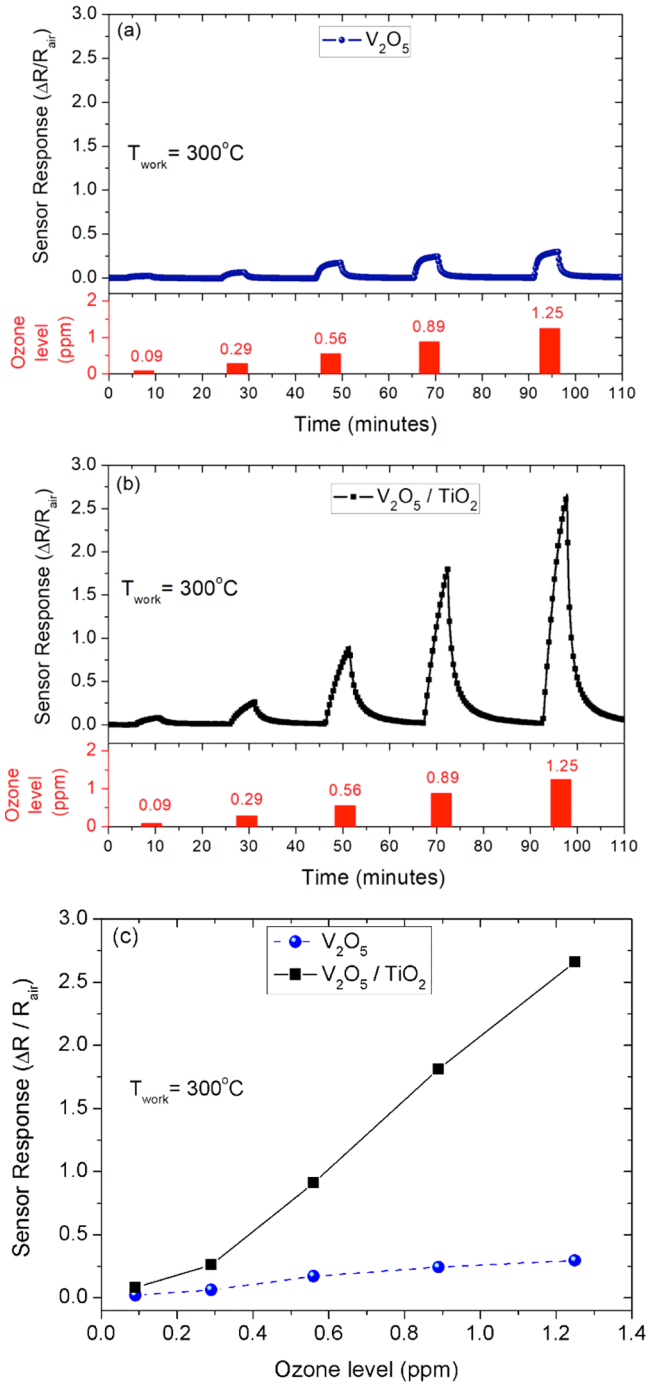

Figure 5. Dynamic response–recovery curves of (a) pristine V_2O_5 and (b) V_2O_5/TiO_2 heterostructure-based sensors to O_3 gas at a working temperature of 300 °C in different levels for 5 min. (c) Sensor response comparison for V_2O_5 and V_2O_5/TiO_2 samples.

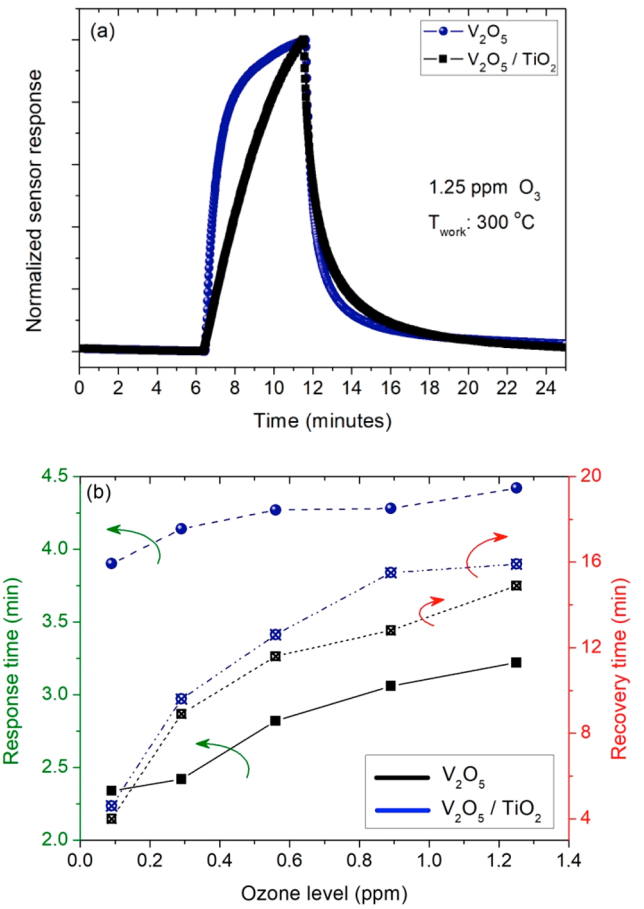

Figure 6. (a) Normalized sensor response of V_2O_5 and V_2O_5/TiO_2 upon an exposure to 1.25 ppm of O_3 at a working temperature of 300 °C. (b) Variation of response and recovery time as a function of ozone levels.

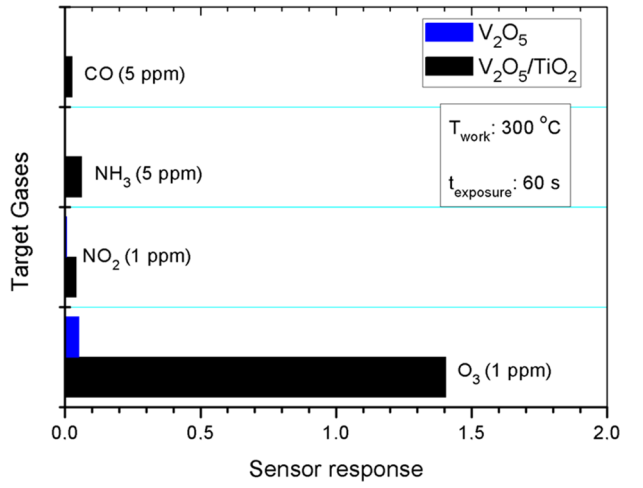

Figure 7. Sensor response comparison between pristine V_2O_5 and V_2O_5/TiO_2 heterostructure exposed to O_3, NO_2, NH_3, and CO gases.

better when exposed to O_3 gas. On the other hand, the pristine V_2O_5 sample exhibited comparable response to all gases evaluated. It is important to highlighted that MOX sensors which have been studied to detect the ozone level in the atmosphere were reported with a low selectivity,[27] or even with a unknown selectivity.[28,35−39] Therefore, we can conclude that this heterostructure is promising for practical applications, as it is capable of detecting subppm ozone levels.

The long-term stability was also evaluated by exposing the sensors three times to 0.29 ppm of O_3 at 300 °C for 30 days, and the results are shown in Figure 8. After consecutive exposures, the sensitivity of V_2O_5/TiO_2 was still higher than that of the pristine sample, demonstrating that these heterostructures have greater potential to detect ozone gases over long periods of time.

In order to understand the better gas-sensing performance of V_2O_5 and V_2O_5/TiO_2 heterostructures, XPS analyses were

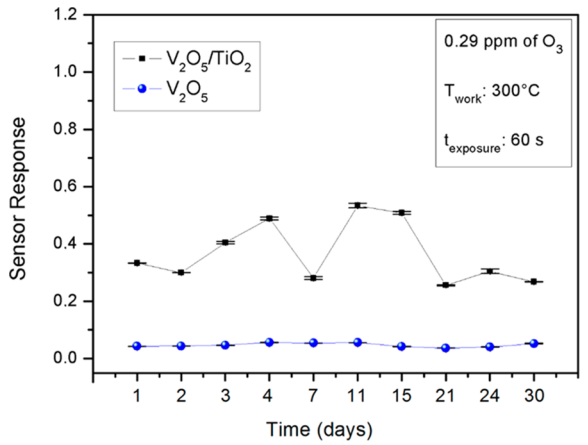

Figure 8. Gas sensor response of both pristine V_2O_5 and V_2O_5/TiO_2 heterostructure upon an exposure to 0.29 ppm of ozone for 30 days.

performed. Due to the lower amount of TiO_2 nanoparticles and its sensing performance, we focused our measurements on the V_2O_5/TiO_2 sample with 25 mol %. Figure 9a shows a typical XPS survey spectrum of the as-obtained V_2O_5 and V_2O_5/TiO_2 (25 mol %) samples. The observed peaks in these spectra only reveals the presence of V, Ti, O, and C. Carbon is a contaminant adsorbed on the sample surface associated to the ambient exposition (according to O 1s XPS analyses). Figure 9b shows a high-resolution Ti 2p XPS, where it is possible to see titanium peaks consisting of Ti $2p_{3/2}$ and Ti $2p_{1/2}$ spectral doublets with binding energies of about 458.5 and 464.3 eV comparable to those reported for titanium dioxide, thus confirming the presence of Ti^{4+} ions.[56] The vanadium−oxygen region in the XPS spectra of such samples is displayed in Figure 9. XPS analyses reveal very similar results for both samples. The V 2p XPS spectra consist of two peaks at 517.5 and 524.9 eV related to spin−orbit components.[57] The deconvolution of the V $2p_{3/2}$ peak into two components at approximately 517.5 and 515.1 eV reveals the presence of multiple vanadium oxidation states, i.e., V^{5+} and V^{4+} ions.[58] The O 1s spectra were deconvoluted into three components, labeled as O 1s(1), O 1s(2), and O 1s(3), as seen in Figure 9d. The main peak at ∼530 eV corresponds to O^{2-} ions connected to metal cations (Ti^{4+} and/or V^{4+}/V^{5+}),[58] while the other two peaks with a binding energy of approximately 531.4 and 532.8 eV are ascribed to hydroxyl groups (OH−) and oxygen bound to organic species and/or water molecules adsorbed in sample surface, respectively.[20,59] Additionally, the O 1s(2) component can also be associated with surface defects or oxygen vacancies.[16] The presence of these oxygen vacancies or defect concentration on the surface of the samples might facilitate the chemisorption process, which could contribute to an improvement of the gas-sensing performance.[16] Comparing the obtained values for the pristine V_2O_5 and V_2O_5/TiO_2 (25

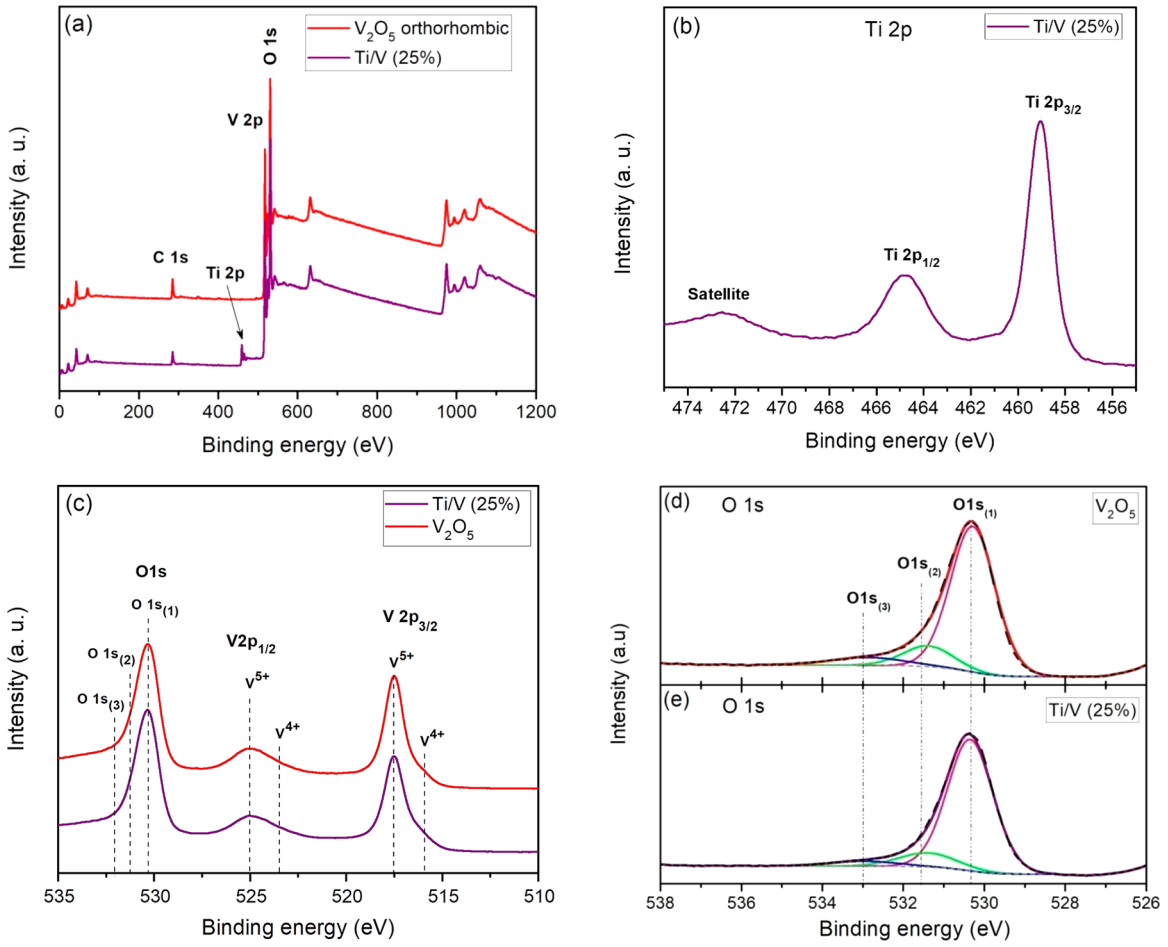

Figure 9. XPS spectra of the V_2O_5 and V_2O_5/TiO_2 (25 mol %) samples. (a) Survey scan; (b) Ti 2p; (c) V 2p and O 1s; (d and e) deconvoluted O 1s XPS spectra.

mol %) heterostructure, the percentage of the O 1s(2) component is quite similar, i.e., approximately 13% and 12%, respectively. Thus, only the presence of oxygen vacancies or defect concentration on the surface does not explain the improvement in the gas-sensing performance.

Several papers have focused their work on gas-sensing performance of heterojunctions.[15,19−24] Recently, our group investigated the gas-sensing properties of a ZnO/SnO_2 heterojunction operated at room temperature under ultraviolet illumination.[21] It was observed that the formation of the heterojunction hinders the charge carrier recombination, which consequently become available for chemisorption processes.[21] Both V_2O_5 and TiO_2 are n-type semiconductors with distinct electronic properties, such as electron affinity (χ),[19,60] work functions (φ),[19,58] and band gaps.[19,20,44,58,61] Based on this, Fu and co-workers proposed a gas-sensing mechanism capable of detecting VOCs for TiO_2-based heterojunctions.[19] According to the authors, when an equilibrium between the semiconductors occurs, the electron transfers from TiO_2 to the lower-energy conduction band of V_2O_5 until their Fermi energy levels become equal.[19] This alignment leads to a band bending after the equilibrium is reached, resulting in the presence of a higher number of electrons in the TiO_2 conduction band.[19] Wang et al. also observed that the formation of n−n type heterojunctions based on TiO_2 and V_2O_5 results in an energy barrier and additional depletion layer at the interfaces, influencing the heterojunction resistance.[20] Concerning O_3 sensing performance, V_2O_5−TiO_2 thin films were already studied by Zhuiykov et al, who observed a low ozone response of the heterostructure attributed to the presence of carbon impurities poisoning active sites on the sample surface, probably related to the sol−gel method employed to obtain the samples.[27] This brings an important advantage, since this method excludes the presence of foreign ions or organic ligands which influence their sensing performance and are often not easily eliminated.[40,41,44,61,62]

Besides having higher sensor performances, the studied V_2O_5/TiO_2 heterostructures present different dynamic curves observed for sensor response, showing that the formation of a heterojunction creates additional actives sites. In this way, the enhanced sensor response of the V_2O_5/TiO_2 heterostructure to O_3 gas can be linked to a two-phase interface synergistic effect induced by effective heterojunctions between V_2O_5 nanowires and TiO_2 nanoparticles. As a matter of fact, the pristine TiO_2 sample was not sensitive toward O_3 gas, considering the O_3 level and working temperatures employed. As the V_2O_5/TiO_2 heterostructure was thermally activated, the modulation of the potential barrier energy starts at the heterojunction interface after the combination of both semiconductors, thus enhancing its gas sensor performance in a mechanism similar to that proposed by different sensors based on heterostructures.[19,20] The ozone sensing mechanism is illustrated by Figure 10. When the samples are exposed to O_3 gas, O_3 molecules are adsorbed and react on their surface according to the equations in Figure 10. Then, the trapped electrons are released, changing the barrier potential at the interface, thus leading to a variation of resistance.

4. CONCLUSION

The structural, electronic, and surface properties of V_2O_5/TiO_2 heterostructures, obtained via hydrothermal route, were studied in detail. HRTEM and EELS mapping analyses confirm the formation of V_2O_5/TiO_2 heterojunctions.

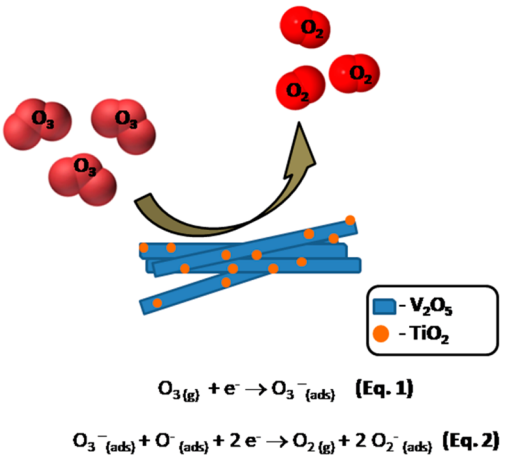

Figure 10. Ozone gas-sensing mechanism of V_2O_5/TiO_2 heterostructures obtained via hydrothermal treatment.

Electrical measurements demonstrated that the ozone sensor response increases considerably as a result of the formation of heterojunctions between V_2O_5 and TiO_2. Such improvement can be attributed to a good separation of charge carriers at the two-phase interface, displaying a synergistic effect that facilitates ozone chemisorption processes. To summarize, the studied samples present very promising gas-sensing properties toward ozone gas with great sensor response, selectivity, and repeatability as well as a subppm range of detection. These results represent a remarkable advance for technological applications in ozone sensing.

■ ASSOCIATED CONTENT

Supporting Information

The Supporting Information is available free of charge on the ACS Publications website at DOI: 10.1021/acsanm.9b00578.

Image of the dynamic gas-sensing chamber used in the sensing experiments; sensor response for pristine V_2O_5 and V_2O_5/TiO_2 heterostructure at 300 °C upon exposure to 0.89 ppm of O_3 gas during 10 min; sensor response of the pristine V_2O_5 and V_2O_5/TiO_2 heterostructures when exposed to 0.29 ppm of O_3 gas as a function of the working temperature; sensor response for pristine V_2O_5 and V_2O_5/TiO_2 (25%mol) heterostructure at 300 °C upon exposure to 0.89 ppm of O_3 gas during 60 s (PDF)

■ AUTHOR INFORMATION

Corresponding Author

*E-mail: w_avansi@ufscar.br.

ORCID

Waldir Avansi, Jr.: 0000-0001-8155-9364

Lúis F. da Silva: 0000-0001-6257-5537

Valmor R. Mastelaro: 0000-0001-9512-4214

Notes

The authors declare no competing financial interest.

■ ACKNOWLEDGMENTS

The authors gratefully acknowledge the financial support of the Brazilian research funding agencies FAPESP (under grant number FAPEP 2013/17639-4, 2013/07296-2, 17/18649-4, and 2017/12437-5), CNPq (311463/2017-7), and CAPES

(Financial Code 001). Transmission electron microscopy (TEM-21464) and X-ray photoelectron spectroscopy (XPS-20607 and XPS-21082) were performed at the LME/LNNano/CNPEM. The electrodes used for the gas-sensing experiments were fabricated in the Laboratory of Microfabrication at the LNNano/CNPEM (Projects LMF-18580). The STEM-EELS and HRTEM measurements were performed in the Advanced Microscopy Laboratory (LMA) at the Institute of Nanoscience of Aragon (INA), University of Zaragoza (Spain). R.A. gratefully acknowledges the support from the Spanish Ministry of Economy and Competitiveness (MAT2016-79776-P) and the Government of Aragon through projct DGA E13_17R (FEDER, EU).

REFERENCES

(1) Zhang, J.; Liu, X. H.; Neri, G.; Pinna, N. Nanostructured Materials for Room-Temperature Gas Sensors. *Adv. Mater.* **2016**, *28* (5), 795−831.

(2) Zhou, X.; Lee, S.; Xu, Z. C.; Yoon, J. Recent Progress on the Development of Chemosensors for Gases. *Chem. Rev.* **2015**, *115* (15), 7944−8000.

(3) Pandey, S.; Goswami, G. K.; Nanda, K. K. Nanocomposite based flexible ultrasensitive resistive gas sensor for chemical reactions studies. *Sci. Rep.* **2013**, *3*, 3.

(4) Pandey, S.; Nanda, K. K. Au Nanocomposite Based Chemiresistive Ammonia Sensor for Health Monitoring. *Acs Sensors* **2016**, *1* (1), 55−62.

(5) Gao, X.; Zhang, T. An overview: Facet-dependent metal oxide semiconductor gas sensors. *Sens. Actuators, B* **2018**, *277*, 604−633.

(6) Schneider, K.; Lubecka, M.; Czapla, A. V_2O_5 thin films for gas sensor applications. *Sens. Actuators, B* **2016**, *236*, 970−977.

(7) Liu, J. F.; Wang, X.; Peng, Q.; Li, Y. D. Vanadium pentoxide nanobelts: Highly selective and stable ethanol sensor materials. *Adv. Mater.* **2005**, *17* (6), 764−767.

(8) Avansi, W.; Maia, L. J. Q.; Ribeiro, C.; Leite, E. R.; Mastelaro, V. R. Local structure study of vanadium pentoxide 1D-nanostructures. *J. Nanopart. Res.* **2011**, *13* (10), 4937−4946.

(9) Huotari, J.; Lappalainen, J.; Puustinen, J.; Spetz, A. L. Gas sensing properties of pulsed laser deposited vanadium oxide thin films with various crystal structures. *Sensors and Actuators B-Chemical* **2013**, *187*, 386−394.

(10) Schneider, K.; Maziarz, W. V_2O_5 Thin Films as Nitrogen Dioxide Sensors. *Sensors* **2018**, *18* (12), 4177.

(11) Vieira, N. C. S.; Avansi, W.; Figueiredo, A.; Mastelaro, V. R.; Zucolotto, V. Potentiometric detection of chemical species by spin-assisted assembly of vanadium pentoxide nanorods. *Sens. Actuators, B* **2016**, *229*, 461−465.

(12) Vieira, N. C. S.; Avansi, W.; Figueiredo, A.; Ribeiro, C.; Mastelaro, V. R.; Guimares, F. E. G. Ion-sensing properties of 1D vanadium pentoxide nanostructures. *Nanoscale Res. Lett.* **2012**, *7*, 1−5.

(13) Yang, Y.; Hong, A. J.; Liang, Y.; Xu, K.; Yu, T.; Shi, J.; Zeng, F. Y.; Qu, Y. H.; Liu, Y. T.; Ding, M. Q.; Zhang, W.; Yuan, C. L. High-energy {001} crystal facets and surface fluorination engineered gas sensing properties of anatase titania nanocrystals. *Appl. Surf. Sci.* **2017**, *423*, 602−610.

(14) Chinh, N. D.; Kim, C.; Kim, D. UV-light-activated H2S gas sensing by a TiO_2 nanoparticulate thin film at room temperature. *J. Alloys Compd.* **2019**, *778*, 247−255.

(15) Miller, D. R.; Akbar, S. A.; Morris, P. A. Nanoscale metal oxide-based heterojunctions for gas sensing: A review. *Sens. Actuators, B* **2014**, *204*, 250−272.

(16) Catto, A. C.; da Silva, L. F.; Bernardi, M. I. B.; Bernardini, S.; Aguir, K.; Longo, E.; Mastelaro, V. R. Local Structure and Surface Properties of $Co_xZn_{1-x}O$ Thin Films for Ozone Gas Sensing. *ACS Appl. Mater. Interfaces* **2016**, *8* (39), 26066−26072.

(17) Barsan, N.; Koziej, D.; Weimar, U. Metal oxide-based gas sensor research: How to? *Sens. Actuators, B* **2007**, *121* (1), 18−35.

(18) Tricoli, A.; Righettoni, M.; Teleki, A. Semiconductor Gas Sensors: Dry Synthesis and Application. *Angew. Chem., Int. Ed.* **2010**, *49* (42), 7632−7659.

(19) Fu, H. T.; Yang, X. H.; An, X. Z.; Fan, W. R.; Jiang, X. C.; Yu, A. B. Experimental and theoretical studies of V_2O_5@TiO_2 core-shell hybrid composites with high gas sensing performance towards ammonia. *Sens. Actuators, B* **2017**, *252*, 103−115.

(20) Wang, Y.; Zhou, Y.; Meng, C. M.; Gao, Z.; Cao, X. X.; Li, X. H.; Xu, L.; Zhu, W. J.; Peng, X. S.; Zhang, B. T.; Lin, Y. F.; Liu, L. X. A high-response ethanol gas sensor based on one-dimensional TiO_2/V_2O_5 branched nanoheterostructures. *Nanotechnology* **2016**, *27* (42), 425503.

(21) da Silva, L. F.; M'Peko, J. C.; Catto, A. C.; Bernardini, S.; Mastelaro, V. R.; Aguir, K.; Ribeiro, C.; Longo, E. UV-enhanced ozone gas sensing response of ZnO-SnO_2 heterojunctions at room temperature. *Sens. Actuators, B* **2017**, *240*, 573−579.

(22) Nayak, A. K.; Ghosh, R.; Santra, S.; Guha, P. K.; Pradhan, D. Hierarchical nanostructured WO_3-SnO_2 for selective sensing of volatile organic compounds. *Nanoscale* **2015**, *7* (29), 12460−12473.

(23) Li, H.; Xie, W. Y.; Liu, B.; Wang, Y. R.; Xiao, S. H.; Duan, X. C.; Li, Q. H.; Wang, T. H. Ultra-fast and highly-sensitive gas sensing arising from thin SnO_2 inner wall supported hierarchical bilayer oxide hollow spheres. *Sens. Actuators, B* **2017**, *240*, 349−357.

(24) Epifani, M.; Diaz, R.; Force, C.; Comini, E.; Andreu, T.; Zamani, R. R.; Arbiol, J.; Siciliano, P.; Faglia, G.; Morante, J. R. Colloidal Counterpart of the TiO_2-Supported V_2O_5 System: A Case Study of Oxide-on-Oxide Deposition by Wet Chemical Techniques. Synthesis, Vanadium Speciation, and Gas-Sensing Enhancement. *J. Phys. Chem. C* **2013**, *117* (40), 20697−20705.

(25) Epifani, M.; Comini, E.; Diaz, R.; Force, C.; Siciliano, P.; Faglia, G. TiO_2 colloidal nanocrystals surface modification by V_2O_5 species: Investigation by Ti-47, Ti-49 MAS-NMR and H-2, CO and NO_2 sensing properties. *Appl. Surf. Sci.* **2015**, *351*, 1169−1173.

(26) Raghu, A. V.; Karuppanan, K. K.; Pullithadathil, B. Highly Sensitive, Temperature-Independent Oxygen Gas Sensor Based on Anatase TiO_2 Nanoparticle Grafted, 2D Mixed Valent VOx Nanoflakelets. *Acs Sensors* **2018**, *3* (9), 1811−1821.

(27) Zhuiykov, S.; Wlodarski, W.; Li, Y. X. Nanocrystalline V_2O_5-TiO_2 thin-films for oxygen sensing prepared by sol-gel process. *Sens. Actuators, B* **2001**, *77* (1−2), 484−490.

(28) da Silva, L. F.; Catto, A. C.; Avansi, W.; Cavalcante, L. S.; Andres, J.; Aguir, K.; Mastelaro, V. R.; Longo, E. A novel ozone gas sensor based on one-dimensional (1D) alpha-Ag_2WO_4 nanostructures. *Nanoscale* **2014**, *6* (8), 4058−4062.

(29) Yang, I. A.; Holz, O.; Jorres, A.; Magnussen, H.; Barton, S. J.; Rodriguez, S.; Cakebread, J. A.; Holloway, J. W.; Holgate, S. T. Association of tumor necrosis factor-alpha polymorphisms and ozone-induced change in lung function. *Am. J. Respir. Crit. Care Med.* **2005**, *171* (2), 171−176.

(30) Holz, O.; Jorres, R. A.; Timm, P.; Mucke, M.; Richter, K.; Koschyk, S.; Magnussen, H. Ozone-induced airway inflammatory changes differ between individuals and are reproducible. *Am. J. Respir. Crit. Care Med.* **1999**, *159* (3), 776−784.

(31) Gauderman, W. J.; Gilliland, G. F.; Vora, H.; Avol, E.; Stram, D.; McConnell, R.; Thomas, D.; Lurmann, F.; Margolis, H. G.; Rappaport, E. B.; Berhane, K.; Peters, J. M. Association between air pollution and lung function growth in Southern California children - Results from a second cohort. *Am. J. Respir. Crit. Care Med.* **2002**, *166* (1), 76−84.

(32) Jorres, R.; Nowak, D.; Magnussen, H. The effect of ozone exposure on allergen responsiveness in subjects with asthma or rhinitis. *American Journal of Respiratory and Critical Care Medicine* **1996**, *153* (1), 56−64.

(33) Nasirian, M.; Lin, Y. P.; Bustillo-Lecompte, C. F.; Mehrvar, M. Enhancement of photocatalytic activity of titanium dioxide using non-metal doping methods under visible light: a review. *Int. J. Environ. Sci. Technol.* **2018**, *15* (9), 2009−2032.

(34) Khan, S.; Cho, H.; Kim, D.; Han, S. S.; Lee, K. H.; Cho, S. H.; Song, T.; Choi, H. Defect engineering toward strong photocatalysis of

Nb-doped anatase TiO_2: Computational predictions and experimental verifications. *Appl. Catal., B* **2017**, *206*, 520−530.
(35) Vallejos, S.; Khatko, V.; Aguir, K.; Ngo, K. A.; Calderer, J.; Gracia, I.; Cane, C.; Llobet, E.; Correig, X. Ozone monitoring by micro-machined sensors with WO_3 sensing films. *Sensors and Actuators B-Chemical* **2007**, *126* (2), 573−578.
(36) Belkacem, W.; Labidi, A.; Guerin, J.; Mliki, N.; Aguir, K. Cobalt nanograins effect on the ozone detection by WO_3 sensors. *Sens. Actuators, B* **2008**, *132* (1), 196−201.
(37) Korotcenkov, G.; Blinov, I.; Ivanov, M.; Stetter, J. R. Ozone sensors on the base of SnO_2 films deposited by spray pyrolysis. *Sens. Actuators, B* **2007**, *120* (2), 679−686.
(38) Catto, A. C.; da Silva, L. F.; Ribeiro, C.; Bernardini, S.; Aguir, K.; Longo, E.; Mastelaro, V. R. An easy method of preparing ozone gas sensors based on ZnO nanorods. *RSC Adv.* **2015**, *5* (25), 19528−19533.
(39) Catto, A. C.; Fiorido, T.; Souza, E. L. S.; Avansi, W.; Andres, J.; Aguir, K.; Longo, E.; Cavalcante, L. S.; da Silva, L. F. Improving the ozone gas-sensing properties of $CuWO_4$ nanoparticles. *J. Alloys Compd.* **2018**, *748*, 411−417.
(40) Avansi, W.; Ribeiro, C.; Leite, E. R.; Mastelaro, V. R. Vanadium Pentoxide Nanostructures: An Effective Control of Morphology and Crystal Structure in Hydrothermal Conditions. *Cryst. Growth Des.* **2009**, *9* (8), 3626−3631.
(41) Avansi, W.; Ribeiro, C.; Leite, E. R.; Mastelaro, V. R. Growth kinetics of vanadium pentoxide nanostructures under hydrothermal conditions. *J. Cryst. Growth* **2010**, *312* (23), 3555−3559.
(42) de Mendonca, V. R.; Ribeiro, C. Influence of TiO_2 morphological parameters in dye photodegradation: A comparative study in peroxo-based synthesis. *Appl. Catal., B* **2011**, *105* (3−4), 298−305.
(43) de Mendonca, V. R.; Avansi, W.; Arenal, R.; Ribeiro, C. A building blocks strategy for preparing photocatalytically active anatase TiO_2/rutile SnO_2 heterostructures by hydrothermal annealing. *J. Colloid Interface Sci.* **2017**, *505*, 454−459.
(44) Avansi, W.; Arenal, R.; de Mendonca, V. R.; Ribeiro, C.; Longo, E. Vanadium-doped TiO_2 anatase nanostructures: the role of V in solid solution formation and its effect on the optical properties. *CrystEngComm* **2014**, *16* (23), 5021−5027.
(45) da Silva, L. F.; Mastelaro, V. R.; Catto, A. C.; Escanhoela, C. A.; Bernardini, S.; Zilio, S. C.; Longo, E.; Aguir, K. Ozone and nitrogen dioxide gas sensor based on a nanostructured $SrTi_{0.85}Fe_{0.15}O_3$ thin film. *J. Alloys Compd.* **2015**, *638*, 374−379.
(46) Egerton, R. *Electron Energy-Loss Spectroscopy in the Electron Microscope*; Springer: 2011.
(47) Deepak, F. L., Mayoral, A., Arenal, R. *Advanced Electron Microscopy: Applications for Nanomaterials*; Springer, 2015.
(48) Panchakarla, L. S.; Lajaunie, L.; Ramasubramaniam, A.; Arenal, R.; Tenne, R. Nanotubes from Oxide-Based Misfit Family: The Case of Calcium Cobalt Oxide. *ACS Nano* **2016**, *10* (6), 6248−6256.
(49) Arenal, R.; March, K.; Ewels, C. P.; Rocquefelte, X.; Kociak, M.; Loiseau, A.; Stephan, O. Atomic Configuration of Nitrogen-Doped Single-Walled Carbon Nanotubes. *Nano Lett.* **2014**, *14* (10), 5509−5516.
(50) Kim, H. J.; Lee, J. H. Highly sensitive and selective gas sensors using p-type oxide semiconductors: Overview. *Sens. Actuators, B* **2014**, *192*, 607−627.
(51) Korotcenkov, G.; Cho, B. K. Ozone measuring: What can limit application of SnO_2-based conductometric gas sensors? *Sens. Actuators, B* **2012**, *161* (1), 28−44.
(52) Joshi, N.; da Silva, L. F.; Jadhav, H. S.; Shimizu, F. M.; Suman, P. H.; M'Peko, J. C.; Orlandi, M. O.; Seo, J. G.; Mastelaro, V. R.; Oliveira, O. N. Yolk-shelled $ZnCo_2O_4$ microspheres: Surface properties and gas sensing application. *Sens. Actuators, B* **2018**, *257*, 906−915.
(53) Zeng, W.; Liu, T. M.; Wang, Z. C. Sensitivity improvement of TiO_2-doped SnO_2 to volatile organic compounds. *Phys. E* **2010**, *43* (2), 633−638.
(54) Korotcenkov, G. Metal oxides for solid-state gas sensors: What determines our choice? *Mater. Sci. Eng., B* **2007**, *139* (1), 1−23.
(55) Maeng, S.; Kim, S. W.; Lee, D. H.; Moon, S. E.; Kim, K. C.; Maiti, A. SnO2 Nanoslab as NO_2 Sensor: Identification of the NO2 Sensing Mechanism on a SnO_2 Surface. *ACS Appl. Mater. Interfaces* **2014**, *6* (1), 357−363.
(56) Lobacheva, O.; Yiu, Y. M.; Chen, N.; Sham, T. K.; Goncharova, L. V. Changes in local surface structure and Sr depletion in Fe-implanted $SrTiO_3$ (001). *Appl. Surf. Sci.* **2017**, *393*, 74−81.
(57) Sun, J. J.; Li, X. Y.; Zhao, Q. D.; Ke, J.; Zhang, D. K. Novel V_2O_5/$BiVO_4$/TiO_2 Nanocomposites with High Visible-Light-Induced Photocatalytic Activity for the Degradation of Toluene. *J. Phys. Chem. C* **2014**, *118* (19), 10113−10121.
(58) Wang, Y.; Su, Y. R.; Qiao, L.; Liu, L. X.; Su, Q.; Zhu, C. Q.; Liu, X. Q. Synthesis of one-dimensional TiO_2/V_2O_5 branched heterostructures and their visible light photocatalytic activity towards Rhodamine B. *Nanotechnology* **2011**, *22* (22), 225702.
(59) Da Silva, L. F.; Lopes, O. F.; Catto, A. C.; Avansi, W.; Bernardi, M. I. B.; Li, M. S.; Ribeiro, C.; Longo, E. Hierarchical growth of ZnO nanorods over SnO_2 seed layer: insights into electronic properties from photocatalytic activity. *RSC Adv.* **2016**, *6* (3), 2112−2118.
(60) Kuruvila, A.; Kidambi, P. R.; Kling, J.; Wagner, J. B.; Robertson, J.; Hofmann, S.; Meyer, J. Organic light emitting diodes with environmentally and thermally stable doped graphene electrodes. *J. Mater. Chem. C* **2014**, *2* (34), 6940−6945.
(61) Avansi, W.; de Mendonca, V. R.; Lopes, O. F.; Ribeiro, C. Vanadium pentoxide 1-D nanostructures applied to dye removal from aqueous systems by coupling adsorption and visible-light photodegradation. *RSC Adv.* **2015**, *5* (16), 12000−12006.
(62) Piquemal, J.-Y.; Briot, E.; Bregeault, J.-M. Preparation of materials in the presence of hydrogen peroxide: from discrete or "zero-dimensional" objects to bulk materials. *Dalton Transactions* **2013**, *42* (1), 29−45.